

PAPER • OPEN ACCESS

Chalcogenide perovskites for photovoltaics: current status and prospects

To cite this article: Devendra Tiwari *et al* 2021 *J. Phys. Energy* **3** 034010

View the [article online](#) for updates and enhancements.



PAPER

OPEN ACCESS

Chalcogenide perovskites for photovoltaics: current status and prospects

RECEIVED
15 January 2021REVISED
23 March 2021ACCEPTED FOR PUBLICATION
31 March 2021PUBLISHED
12 May 2021Devendra Tiwari^{1,2} , Oliver S Hutter¹ and Giulia Longo^{1,*} ¹ Mathematics, Physics and Electrical Engineering, Northumbria University, Ellison place, Newcastle upon Tyne NE1 8ST, United Kingdom² School of Chemistry, University of Bristol, Bristol BS8 1TS, United Kingdom

* Author to whom any correspondence should be addressed.

E-mail: g.longo@northumbria.ac.uk**Keywords:** lead-free perovskite, chalcogenide perovskites, photovoltaic applications, novel materialsOriginal content from this work may be used under the terms of the [Creative Commons Attribution 4.0 licence](https://creativecommons.org/licenses/by/4.0/).

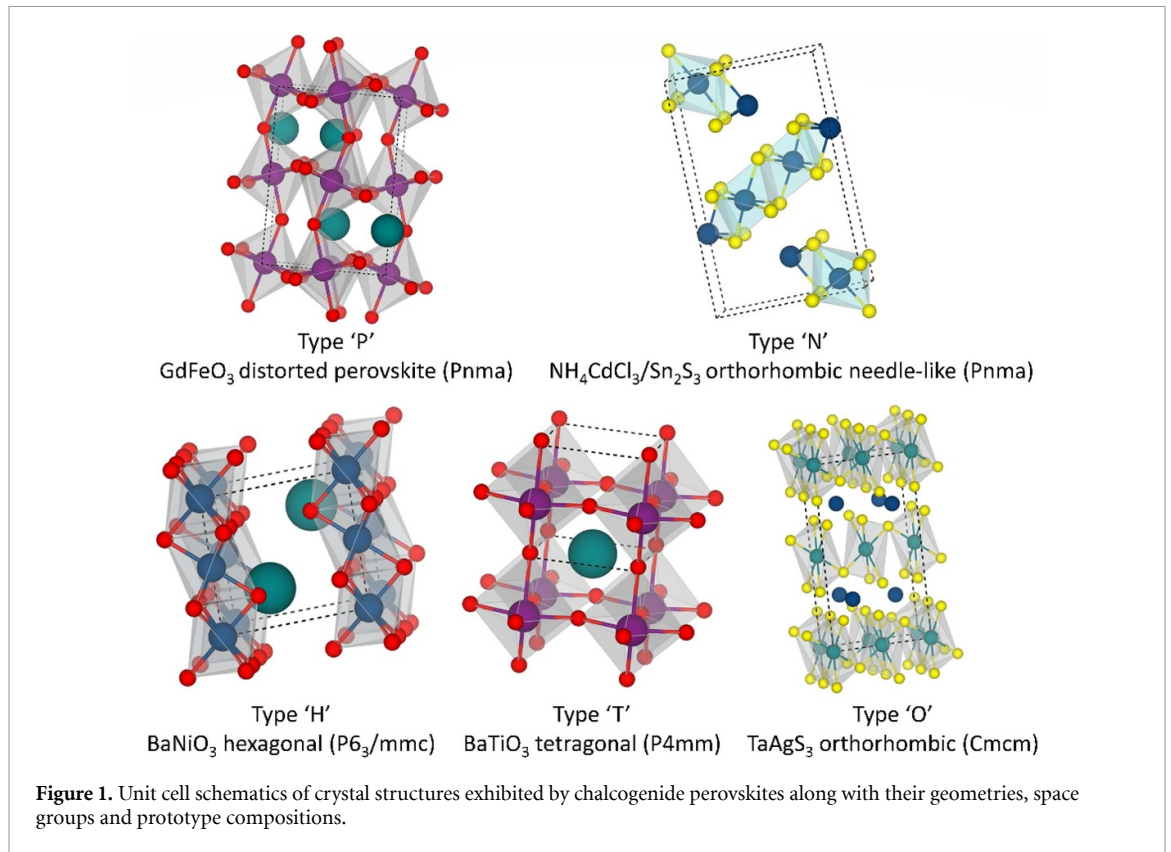
Any further distribution of this work must maintain attribution to the author(s) and the title of the work, journal citation and DOI.

**Abstract**

Chalcogenide perovskite materials are anticipated to have favourable structural, optical and electronic characteristics for solar energy conversion, yet experimental verification of the numerous computational studies is still lacking. In this perspective we summarise and critically review the computational and synthetic achievements, whilst suggesting new pathways for achieving the goal of developing this exiting class of materials. Greater knowledge of phase chemistry would allow the realisation of bandgap engineering through mixed cation and anion compositions. Combining this with fabrication and characterisation of thin films could yield promising new tailored materials for photovoltaic absorbers in the near future.

Lead-based organic-inorganic hybrid perovskites have gained increasing interest in recent years, climbing the photovoltaic efficiency charts and reaching performances comparable to more mature technologies, such as crystalline silicon [1–6]. Despite the excellent photophysical properties and the impressive improvements in device performance, hybrid lead halide perovskites (such as $\text{CH}_3\text{NH}_3\text{PbI}_3$) suffer from poor ambient stability. Small organic molecules like methylammonium result in degradation due to humidity, oxygen or heat exposure. Substitution with larger organic components (such as formamidinium) or inorganic cations (such as Cs) partially improves the environmental stability, whilst introducing phase instability, thus requiring complex compositions and rigorous encapsulation [7–12]. Additionally, the presence of lead in the material composition raises toxicity concerns. Regardless of differing opinions on the balance of lead's hazard and benefits for photovoltaics [13–17], it is indisputable that long-living, lead-free and efficient alternatives are highly desirable. Consequently, the search for environmentally friendly, stable, and equally efficient perovskite substitutes has recently garnered increasing interest from the scientific community. Several options have been examined, such as halide perovskites with Sn^{2+} or Ge^{2+} [18], halide double-perovskites ($\text{A}_2\text{B}'\text{B}''\text{X}_6$) [19], vacancy ordered perovskites (A_2BX_6) [20], and chalcogenide perovskites (ABCh_3) [21–23]. Among them, chalcogenide perovskites (perovskites with oxygen, sulphur or selenium as anions) can serve as promising alternatives consisting of non-toxic and abundant elements. Many recent reports employing computational screening and density functional theory (DFT) calculations have predicted desirable photovoltaic (PV) absorber properties for chalcogenide perovskite materials. As will be elaborated in this review, chalcogenide perovskites offer similar optoelectronic properties to the efficient lead-based perovskites due to similar structural features. This includes strong absorption in the solar spectrum and electronic structures characteristic of facile charge-transport. Above all, chalcogenide perovskites offer a high degree of thermodynamic and atmospheric stability as is usually demonstrated in other inorganic chalcogenides prevalent in PV.

As highlighted in this work, despite the prediction of many chalcogenide perovskites based on S/Se, much of the synthetic efforts have been directed to the fabrication of oxide perovskite materials that have large bandgaps due to the less electronegative or polarisable O^{2-} anion. They are thus not of strong interest as absorber materials for solar energy conversion [24]. In this perspective, we present a critical review of the state-of-the-art in chalcogenide perovskites primarily based on S/Se anions, including the analysis of



structural, optical and electronic characterisations as well as synthesis and attempts at device fabrication. We believe these S/Se based chalcogenide perovskites urgently require a more concerted and interdisciplinary experimental effort to unlock their potential as next-generation sustainable PV absorbers. Based on this discussion, we recommend the most promising directions for future research, namely an emphasis on depositing materials in thin-film form and on the formation of solid-state intermediate alloys, allowing bandgap engineering and thermodynamic stability.

1. Structure and composition of chalcogenide perovskites

Perovskites are crystalline materials characterised by the chemical formula ABY_3 and a generally cubic or orthorhombic lattice, the prototype being $CaTiO_3$. In this work, for clarity, we have referred to Y as general anions, X as halide anions, and Ch as chalcogenide anions. To form a chalcogenide perovskite (i.e. $Y = O^{2-}$, S^{2-} or Se^{2-}), A must be a large cation with the 2+ oxidation state, while B should be a tetravalent cation. Considering this, the immediate choice for the A-site falls upon the alkaline earth elements. However, many transition d-block and f-block elements as well as group 14 elements can also exhibit a 2+ oxidation state, and could theoretically be used as A-site elements. Tetravalent candidate elements for the B-site are numerous, the majority of which belong to the d-block, and even some f and p-block elements also present a 4+ oxidation state.

Within these constraints, there are 3744 possible elemental sets that theoretically form a chalcogenide perovskite [23]. However, only a limited number of these compositions are thermodynamically stable and would crystallise in the desired cubic or pseudo-cubic perovskite structure (figure 1). Based on purely geometrical considerations, it is possible to predict both the stability and formability of a particular perovskite form by using the ionic radii of the atoms in its composition to calculate the Goldschmidt tolerance factor (t) and the octahedral factor (μ) [25–27], which are expressed as:

$$t = \frac{(r_A + r_Y)}{\sqrt{2}(r_B + r_Y)}$$

$$\mu = \frac{r_B}{r_Y}$$

Table 1. AB_3 and $ABSe_3$ calculated octahedral factors for 4+ oxidation state B cations. Compositions that should form a perovskite structure are shown in black ($\mu \geq 0.38$), with elemental combinations that could be stabilized as a perovskite phase through compositional engineering shown in blue ($\mu = 0.36-0.37$). Elemental combinations that do not produce a perovskite structure are shown in grey ($\mu \leq 0.35$). Note that for both B and Y, Shannon ionic radii with a coordination number of VI have been used.

d block	p block		f block				
	S	Se	S	Se			
Ti	0.33	0.31	Si	0.22	Ce	0.47	0.44
Zr	0.39	0.36	Ge	0.29	Th	0.51	0.47
Hf	0.39	0.36	Sn	0.38	Pr	0.46	0.43
V	0.32	0.29	Pb	0.42	Pa	0.49	0.45
Nb	0.37	0.34	Te	0.53	U	0.48	0.45
Ta	0.37	0.34	Po	0.51	Np	0.47	0.44
Cr	0.30	0.28			Pu	0.47	0.43
Mo	0.35	0.33			Am	0.46	0.43
W	0.36	0.33			Cm	0.46	0.43
Mn	0.29	0.27			Tb	0.41	0.38
Tc	0.35	0.33			Bk	0.45	0.42
Re	0.34	0.32			Cf	0.45	0.41
Fe	0.32	0.30					
Ru	0.34	0.31					
Os	0.34	0.32					
Co	0.29	0.27					
Rh	0.33	0.30					
Ir	0.34	0.32					
Ni	0.26	0.24					
Pd	0.33	0.31					
Pt	0.34	0.32					

where r_A , r_B and r_Y are the ionic radii for A-site cation, B-cation and Y-anion respectively. From the values of t and μ , it is possible to predict the most stable form. Figure 1 illustrates the five different possible crystal structures for these chalcogenide materials.

Cubic perovskites are formed when $0.91 \leq t \leq 1$ and $\mu \geq 0.41$, distorted perovskites with an orthorhombic structure are obtained when $0.71 \leq t < 0.91$ and $\mu \geq 0.41$, and non-perovskites (tetragonal, hexagonal or orthorhombic with needle-like structures) are formed when $t > 1$, $t < 0.71$, or $\mu < 0.41$ [25, 28]. However, these boundaries are only indicative, as they vary depending on material composition [29] and the specific definition of ionic radius used [30–33]. In fact, several refinements of t and μ have been suggested [29, 32, 34]. Nevertheless, t and μ can still be useful for initial sifting of possible new perovskites, and indeed have been widely used to assess the formability of chalcogenide perovskites [29, 35, 36]. However, to get consistent predictions, it is proposed herein to use the tolerance factor in conjunction with the octahedral factor, while the literature often shows reports solely using the tolerance factor. The exceptional carrier-transport and light-absorption properties of hybrid lead halide perovskites arise from the terminal connected network of PbX_6 octahedra [37]. Therefore, to instil similar electronic features in chalcogenide perovskites, it is imperative to preserve similar coordination geometry around the B-site atom which is better indicated by the octahedral factor.

Table 1 presents calculated octahedral factors for $ABCh_3$ perovskites (excluding oxygen, see above) for all possible 4+ oxidation state B-cations. Despite values of μ below 0.41 usually being considered as an indicator of a non-perovskite structure, for this work, the acceptable octahedral values have been extended to $\mu \geq 0.36$ based upon experimental results. For example, $BaZrS_3$ has been synthesized in a distorted perovskite structure despite the fact that $\mu = 0.39$ [22, 38]. Values of μ between 0.36 and 0.39 have been included to consider perovskites that could be stabilised by using mixed B and Y cations, as previously reported for $BaZr_xTi_{1-x}S_3$ and $BaZr(S_xSe_{1-x})_3$ [37, 39]. Among the possible 21 B elements selected under these criteria, rare tellurium and radioactive polonium will not be considered in this work. F block elements are excluded for similar reasons. Lead (Pb) remains in the list as it is useful for characterization and comparison between halogen and chalcogenide perovskites. Consequently, the number of B elements is reduced to 7.

Additional filtering on the possible compounds is introduced through the tolerance factor (t), as shown in table 2. The ionic radii of A used in the calculation refer to the XII coordination number. For d-group A-site cations, the ionic radii for the XII coordination number have been calculated as reported elsewhere [30]. Table 2 employs a slightly greater threshold for t of 0.76 compared to the theoretical 0.71 in order to accommodate larger octahedral factors as needed for stable perovskites. Additionally, the elements Ra, Pd, Pt,

Table 2. Tolerance factors for the chalcogenide perovskites compositions. Experimentally evaluated (black) and calculated (white) crystalline structures are indicated as: P = distorted perovskite structure, N= orthorhombic needle-like structure, H = hexagonal structure, T = tetragonal structure, and O = orthorhombic structure. These crystal structures are shown in figure 1. The B elements reported in blue are the elements with a low octahedral factor of $0.36 < \mu < 0.39$.

	S						Se			Key		
	Zr	Hf	Nb	Ta	W	Sn	Pb	Zr	Hf	Pb	t	
Ca	p ²²										0.96–1.0	
Sr	N ²² , p ³⁷		p ^{37,40}								N ⁴¹	0.91–0.95
Ba	p ^{22,37,38,2,43}		p ^{37,40}		H		H		N ⁴¹			0.86–0.90
Ti											0.81–0.85	
V											0.76–0.80	
Mn												
Fe												
Co												
Ag			O									
Zn												
Pb	N ⁴⁴		N ⁴⁵		T ⁴⁶		T ⁴⁶		N ⁴¹			

Cd and Hg, despite featuring a 2+ oxidation state and suitable tolerance factors, are not considered due to either radioactivity, toxicity, low-abundance, or high-costs.

Table 2 also highlights experimentally evaluated structures, demonstrating the extremely limited number of synthesized materials compared to potential compositions. As detailed later in this perspective, this disparity derives from the significantly more challenging synthesis of chalcogenide perovskites compared to lead-based halide materials. The combined use of both μ and t provides more realistic prospects of stable new chalcogenide perovskite compositions, including mixed B and mixed Ch structures. However, this theoretical selection should be corroborated by experimental structural data for any discrepancies, as exemplified by PbZrS₃, which presents a needle-like orthorhombic structure, despite having $\mu = 0.39$ and $0.91 < t < 0.95$, and consequently a predicted perovskite structure. Additionally, the geometrical factors presented in table 2 do not consider the formation of competing phases during synthesis, which must be carefully evaluated before dedicating a great experimental effort. As such, phase diagrams for the most salient candidates identified in this work would be incredibly useful for predicting compositional stability windows and guiding synthetic routes.

2. Optoelectronic properties of chalcogenide perovskites

With the advent of large-scale materials discovery programs such as the Materials Project [47] and NoMAD [48], it has become possible to construct extensive maps of composition and phases [23]. However, it is worth noting that discrepancies exist between databases, originating from differences in the numerical implementation of DFT or associated algorithms [49, 50]. Formation energies are often used to benchmark different DFT implementations but do not ensure the accuracy of electronic structure parameters (e.g. bandgaps and effective masses) and optical properties (e.g. absorption coefficients) [51–53]. Thus, stricter benchmarking procedures and experimental verification are required [54]. Chalcogenide perovskites exemplify this issue well as most of the reported literature is computational, with very few synthetic reports.

Similar to lead hybrid halide perovskites, the composition of the band edges in chalcogenide perovskites is dictated solely by the B-site cation d-states and chalcogen p-states, while the A-site cation bands appear localised and deep [55, 56]. An additional similarity to the lead halide perovskites is the degree of covalency in the B-Ch bonds achieved due to the reduced electronegativity difference between the B-site metal and the chalcogen. This is in stark contrast to ferroelectric oxides, which exhibit UV-bandgaps due to the polar bonding nature [57, 58]. The increased covalency of chalcogenide perovskites also manifests in larger band-dispersions and thus small effective masses ($<0.5 m_e$), which indicate fast carrier-mobilities. This can be seen in table 3, where optical and transport parameters (bandgap, absorption coefficient and effective masses) calculated using hybrid functional DFT calculations are listed. Calculations show that chalcogenide perovskites present ultra-high absorption coefficients of $>10^5 \text{ cm}^{-1}$ at the absorption onset, which can reduce the need for long diffusion lengths and translate into high photovoltaic performance [37].

BaZrS₃ has to date received more attention than any other chalcogenide perovskite, which is understandable given its relatively low bandgap. The strong absorption of BaZrS₃ primarily arises from the S-p to Zr-d transitions which, combined with the large joint density of states at the valence band maximum, leads to a much larger transition probability [37, 59]. This is unique for ABS₃ materials and in contrast to hybrid halide perovskites where transitions originate from or to hybridised bands [59]. The experimentally

Table 3. Summary of calculated optoelectronic parameters of selected chalcogenide perovskites, including bandgap (E_g), absorption coefficient (α) and effective masses (m^*) [24, 35, 37].

		BaZrS ₃	BaZrSe ₃	SrZrS ₃	CaZrS ₃	BaHfS ₃	SrHfS ₃	SrSnS ₃	CaSnS ₃
E_g (eV)	Direct	1.81	1.44	1.46	2.48	1.31	1.12	1.56	1.58
	Indirect	1.81	1.01	1.46	2.48	1.31	1.12		1.98
α (cm ⁻¹)		>10 ⁵		>10 ⁵		>10 ⁵	>10 ⁵	>10 ⁵	
m^*	e ⁻	0.43		0.79	0.41	0.94	0.23	0.5	0.31
	h ⁺	0.75	0.82	0.34	0.22	0.35	0.27	0.33	0.64

observed and calculated sharp absorption edge of BaZrS₃ indicates a low density of tail states with Urbach energies of 28 meV, comparable to that of high-efficiency CH₃NH₃PbI₃ [60]. Similarly, the photoluminescence peaks for BaZrS₃ and some other ABS₃ compositions show sharp peaks with small Stoke-shifts from the respective bandgaps and decent yields at initial stages of development. This in-principle is a harbinger for high open-circuit voltages [61].

Whilst the bandgap of BaZrS₃ (~1.8 eV) is too high for single-junction PV devices, it may be suitable for tandem applications. Alloying with other cations and anions has therefore been explored to lower the bandgap for single-junction applications [37, 39, 56, 62]. In particular, Ti substitution on the Zr-site and Se mixing with S have shown desired results. Titanium inclusion is predicted to lower the bandgap linearly and more significantly than selenisation, which shows bowing [56]. For example, BaZr_{0.75}Ti_{0.25}S₃ is calculated to have a bandgap of 1.43 eV, which is near-optimal according to the Shockley-Queisser limit [56]. Unfortunately, BaTiS₃ forms a hexagonal structure with edge-sharing octahedra. As a result, Ti alloying over 5 atomic % can induce a structural transition with the predominant formation of needle-like structures and a significant broadening of its absorption edge with an increased Urbach energy, resulting in a high-density of voltage curtailing tail states [37]. However, recent reports showed that even a small amount of Ti (around 5 atomic %) could effectively reduce the bandgap up to 300 meV, confirming the potential of bandgap engineering through B-element alloying [37, 39]. On the other hand, a higher quantity of selenium can be introduced into sulphide perovskites without the appearance of secondary phases. Nishigaki *et al* prepared phase-pure BaZr(S_{0.6}Se_{0.4})₃ that presented a 180 meV bandgap reduction compared to BaZrS₃ [37]. Similarly to lead-based halide perovskites, bandgap engineering through compositional modification is therefore a reliable (and virtually unexplored) path to optimize the optoelectronic features of chalcogenide perovskites for the desired applications.

Despite various first-principles electronic structure calculations of BaZrS₃ and other ABCh₃ materials estimating excellent optical and transport parameters as photovoltaic absorbers, the actual performance may be dominated by the nature of the defect chemistry. Meng *et al* have calculated the formation energies and transition energy levels of different native point defects of Ba(Zr,Ti)S₃ under the different synthesis conditions spanned by the theoretical ternary phase diagram [56]. Only 5 out of the possible 12 defects, namely (S_i, S_{Zr}, S_{Ba}, Zr_i and Zr_S) form deep levels within the bandgap with activation energies >350 meV and out of these S_{Ba} and S_i become the most probable defects under S-rich conditions. In contrast, Zr-rich conditions will lead to the formation of only shallow defects, which unfortunately could result in high-levels of donor densities and small depletion widths. Thus, the ideal growth conditions for high-quality BaZrS₃ will be near-stoichiometric as is experimentally supported by the better photoluminescence response [38]. However, this is the only study on defects in chalcogenide perovskites, and a more generalised study, including different compositions, would be extremely useful for progression of the field.

As all of the reported computational works to date have essentially focused on Zr and Hf perovskites [63], it would be interesting to explore more mixed B-cation compositions from the possibilities suggested in table 1. If mixed Zr-Ti compositions could be stabilised up to a 5 atomic % in Ti, despite the much lower octahedral factor of Ti, it is likely that other B elements could also be stabilised, providing a route to reduce and carefully engineer the bandgap of chalcogenide perovskites.

3. Synthesis of chalcogenide perovskites

Clearly, one of the biggest challenges with chalcogenide perovskites is represented by their synthesis. So far, few sulphide compositions have been prepared, as listed in table 2, while selenide perovskites have not yet been obtained, with the exception of the mixed sulphide and selenide composition previously discussed. The majority of the experimentally prepared compositions listed in table 2 are synthesised through solid-state reactions. In this method, the elemental or binary-chalcogenide precursors are sealed in an ampoule and heated at high temperature for several hours or days. Through this process, both distorted perovskites (BaZrS₃ [37], SrZrS₃ [37], BaHfS₃ [40], SrHfS₃ [40], BaZr(S_{1-x}Se_x)₃ [37]) and non-perovskite

materials (PbHfS₃ [45], PbTaS₃ [46], PbNbS₃ [64],) have been prepared. Variants of this technique have also been reported, such as solid-state synthesis at high pressure (used for the synthesis of PbZrS₃ [44], BaSnS₃ [41], SrSnS₃ [41] and PbSnS₃ [41]). Another interesting variant consists of the solid-state synthesis of the oxide perovskites followed by sulfurization through CS₂ (used for the synthesis of CaZrS₃) [22, 37, 39]. It is important to stress that the synthetic conditions play a fundamental role in the formability and in the phase determination of the desired material. In fact, the mixed composition Ba(Zr_xTi_{1-x})S₃ could be achieved only with the oxide perovskite sulfurization with CS₂ [37, 39], while the direct synthesis through the solid-state reaction of the sulphide precursors was ineffective [56]. On the contrary, using the CS₂ variant for the synthesis of SrZrS₃ resulted in a non-perovskite structure [22], while the standard solid-state reaction produced SrZrS₃ in a distorted perovskite structure [37].

Generally, experimental characterization of the optoelectronic properties of chalcogenide perovskites is in good agreement with the calculated predictions from computational analysis. It is worth noting however, that despite the limited number of synthetic reports, there is already some variability in the measured values. For example, the measured bandgap of BaZrS₃ varies between 1.70 eV and 1.94 eV [37, 39]. Similarly, the recorded photoluminescence wavelength also varies from 1.9 eV to less than 1.7 eV [22, 42]. Rather than a specific synthesis driven bandgap modification, these discrepancies should be attributed to the different nature of the characterized samples (nanoparticles, thin films and powders) and to the chosen method of evaluation, such as Tauc or Kubelka-Munk analysis.

The comparison of the synthetic procedures followed for the preparation of BaZrS₃ revealed a common problem of the direct synthesis of chalcogenide perovskites: the formation of undesired products such as binary sulphides or binary oxides [37, 38]. It appears that BaZrS₃ produced by direct reaction of disulphide precursors or elemental precursors is more prone to oxidation compared to material created from the conversion of the oxide perovskite (BaZrO₃) with CS₂ [22] or with the aid of a catalyst like I₂ [42], as these do not reveal any secondary phases. This appears not to be influenced by the synthetic environment (oxygen-rich or inert atmosphere) but rather by elemental stoichiometry, as suggested by Comparotto *et al*, who attribute the unwanted phase formation to the presence of S-rich regions in the material [38]. However, due to the lack of information about the formation process and kinetics, it is difficult to speculate on the optimum synthetic procedure to follow. The high temperature reported for the synthesis of BaZrS₃ and other chalcogenide compounds suggests the presence of a high energetic barrier for the formation and nucleation of this compound, which is likely to be the reason for its high stability. The understanding of the thermodynamics and kinetics of the formation reaction is therefore a fundamental and missing step for the optimization of this material for energy applications.

The very high temperatures used to obtain crystalline and phase pure materials represent another important hurdle to overcome for the implementation of chalcogenide perovskites in optoelectronic devices. In fact, high-temperature processes are incompatible with the majority of thin-film device processes. Among the perovskite compositions we have discussed so far, only BaZrS₃ has been prepared in thin film form. Comparotto *et al* deposited thin films of BaZrS₃ through sputtering at ambient temperature, but high-temperature annealing of the deposited film was still needed to improve the crystallinity of the material [38]. Similarly, Wei *et al* prepared thin films of BaZrS₃ by sulfurization at high temperature of pulsed laser deposited films of BaZrO₃ [43]. They also prepared a photodetector and evaluated the photoresponse and the electrical behaviour of the material. They identified an n-type conductivity which is probably linked to sulphur vacancies and good carrier mobility of almost 14 cm² V s⁻¹. Unfortunately, the sulfurization temperatures used to prepare the photodetector makes the process unsuitable for the majority of optoelectronic devices. More recently, Ravi *et al* prepared solution-processed thin films using a colloidal dispersion of solid-state synthesized BaZrS₃. Using low-temperature annealing, the chalcogenide perovskite thin films were then implemented in working thin film transistors [42]. The results reveal that the BaZrS₃ nanocrystals show an ambipolar transistor behaviour, and evaluated a hole mobility three times higher than the electron mobility, but still very low (0.059 and 0.017 cm² V s⁻¹ respectively). This is likely due to the low grain size obtained with the nanoparticle processing with low temperature treatments. However, the lower electron mobility compared to hole mobility is in agreement with the high density of donor states evaluated in Wei's work, supporting the hypothesis of a n-type conductivity [39]. To the best of our knowledge, these are the only reports of working thin film optoelectronic devices based on chalcogenide perovskites. Photovoltaic devices based on evaporated LaYS₃ thin films have been reported, but no photocurrent was detected [65]. The reason for the lack of functioning photovoltaic devices could be due to the use of unsuitable partner layers, which is to be expected from a totally new class of materials. In addition to this, synthetic reports are often for bulk materials, and transitioning to thin films of high enough quality for use in photovoltaic devices is a complex task.

From this overview of chalcogenide material synthetic achievements, it is clear that major effort should be dedicated to the material synthesis and thin film deposition of these materials. This goal should be

pursued not only for the preparation of devices, but also to achieve novel compositions, as in the case for mixed Zr-Ti perovskites. Inspiration should be taken from photovoltaic materials with more developed synthesis and deposition routes such as CIGS ($\text{Cu}(\text{In,Ga})\text{Se}_2$), CdS and CZTS ($\text{Cu}_2\text{ZnSnS}_4$), or materials where initial efficiency rises have been more forthcoming like Sb_2Se_3 . From this point of view, thin film growth based on sputtering, e-beam, and vapour deposition appear the most promising routes to achieve thin films of chalcogenide perovskites. However, this does not mean that synthesis of bulk materials should be neglected, as this is important from both a fundamental characterization point of view and for the development of innovative deposition techniques. For example, bulk materials prepared through solid-state synthesis methods could be deposited through flash evaporation [66–69], pulsed laser deposition [70–74], or through solution processing if previously dispersed in colloidal form. Although chalcogen loss does not appear to be an issue for some materials such as BaZrS_3 , which is very thermally stable, it may cause problems for other chalcogen perovskites or with specific deposition methods. This problem has been observed for other chalcogenide absorber materials, such as CZTS, CIGS and Sb_2S_3 [75–78]. In these materials, the volatility of the chalcogenide at elevated temperatures and reduced pressure is problematic as stoichiometric films are often required to reduce defect density. Chalcogen loss is usually minimised by depositing and cooling under an inert atmosphere instead of vacuum and the use of rapid deposition rates. Post growth treatments can also be utilised to try and reverse this chalcogen loss [75–78]. High-temperature annealing for high crystallinity could be replaced by photonic curing [79–82] or solvent assisted recrystallization. The possible combinations are abundant, especially if a multidisciplinary approach that includes inorganic chemistry, material science and device engineering is followed.

4. Conclusions

In this perspective, we have summarized the computational and synthetic achievements and reviewed the structural, optical and electronic properties of chalcogenide perovskites. The computational studies consistently indicate the existence of a variety of stable chalcogenide perovskites with bandgaps and high absorption coefficients suitable for single-junction PV devices. Further, detailed first-principles studies on some of these chalcogenide perovskites also show the shallow nature of point defects and conclude the possibility of fine-tuning the optical and transport properties by the B-cation and anion mixing. Despite these numerous calculations and the features reported, the lack of experimental verification still leaves many open questions and remaining doubt. In this work, we have proposed future directions for the field, highlighting that a focus on the preparation of chalcogenide perovskites is urgently required, with a specific interest in a better understanding of phase chemistry to achieve mixed cation and anion compositions, which show the most significant promise. Specifically, we suggest an exploration of mixed B-cation compositions as listed in table 1 because the vast majority of the computational studies to date have focused on Zr and Hf perovskites. Bandgap engineering in chalcogenide perovskites is shown to be feasible through careful compositional control and should be widened through computation and experimentation to include a broader range of compositions, as identified here. Further fabrication and characterisation of thin films would offer an important step in bridging the gap between the bulk and thin film properties, opening up opportunities for tailored materials for photovoltaic applications.

Data availability statement

No new data were created or analysed in this study.

Acknowledgments

The authors acknowledge Engineering and Physical Sciences Research Council for the financial support (EPSRC ReNU project, EP/S023836/1 and EPSRC North East Centre for Energy Materials, EP/R021503/1). The authors would also like to thank Lucy Whalley for valuable discussions.

ORCID iDs

Devendra Tiwari  <https://orcid.org/0000-0001-8225-0000>

Oliver S Hutter  <https://orcid.org/0000-0002-8838-8956>

Giulia Longo  <https://orcid.org/0000-0002-1163-1110>

References

- [1] Kojima A, Teshima K, Shirai Y and Miyasaka T 2009 Organometal halide perovskites as visible-light sensitizers for photovoltaic cells *J. Am. Chem. Soc.* **131** 6050–1
- [2] Lee M M, Teuscher J, Miyasaka T, Murakami T N and Snaith H J 2012 Efficient hybrid solar cells based on meso-superstructured organometal halide perovskites *Science* **338** 643–8
- [3] Liu M, Johnston M B and Snaith H J 2013 Efficient planar heterojunction perovskite solar cells by vapour deposition *Nature* **501** 395–8
- [4] McMeekin D P et al 2016 A mixed-cation lead mixed-halide perovskite absorber for tandem solar cells *Science* **351** 151–5
- [5] Saliba M et al 2016 Cesium-containing triple cation perovskite solar cells: improved stability, reproducibility and high efficiency *Energy Environ. Sci.* **9** 1989–97
- [6] Jung E H, Jeon N J, Park E Y, Moon C S, Shin T J, Yang T-Y, Noh J H and Seo J 2019 Efficient, stable and scalable perovskite solar cells using poly(3-hexylthiophene) *Nature* **567** 511–5
- [7] Stoumpos C C, Malliakas C D and Kanatzidis M G 2013 Organic tin and lead iodide perovskites with organic cations: unique semiconductors, with phase transitions and near-infrared photoluminescent properties *Inorg. Chem.* **52** 9019–38
- [8] Eperon G E, Paternò G M, Sutton R J, Zampetti A, Haghighirad A A, Cacialli F and Snaith H J 2015 Inorganic caesium lead iodide perovskite solar cells *J. Mater. Chem. A* **3** 19688–95
- [9] Zheng X, Wu C, Jha S K, Li Z, Zhu K and Priya S 2016 Improved phase stability of formamidinium lead triiodide perovskite by strain relaxation *ACS Energy Lett.* **1** 1014–20
- [10] Han Q et al 2016 Single crystal formamidinium lead iodide (FAPbI₃): insight into the structural, optical, and electrical properties *Adv. Mater.* **28** 2253–8
- [11] Zhou Y and Zhao Y 2019 Chemical stability and instability of inorganic halide perovskites *Energy Environ. Sci.* **12** 1495–511
- [12] Park B and Seok S I 2019 Intrinsic instability of inorganic–organic hybrid halide perovskite materials *Adv. Mater.* **31** 1–17
- [13] Li J et al 2020 Biological impact of lead from halide perovskites reveals the risk of introducing a safe threshold *Nat. Commun.* **11** 1–5
- [14] Abate A 2017 Perovskite solar cells go lead free *Joule* **1** 659–64
- [15] Billen P, Leccisi E, Dastidar S, Li S, Lobaton L, Spatari S, Fafarman A T, Fthenakis V M and Baxter J B 2019 Comparative evaluation of lead emissions and toxicity potential in the life cycle of lead halide perovskite photovoltaics *Energy* **166** 1089–96
- [16] Celik I, Song Z, Cimaroli A J, Yan Y, Heben M J and Apul D 2016 Life cycle assessment (LCA) of perovskite PV cells projected from lab to fab *Sol. Energy Mater. Sol. Cells* **156** 157–69
- [17] Babayigit A, Ethirajan A, Muller M and Conings B 2016 Toxicity of organometal halide perovskite solar cells *Nat. Mater.* **15** 247–51
- [18] Nasti G and Abate A 2019 Tin halide perovskite (ASnX₃) solar cells: a comprehensive guide toward the highest power conversion efficiency *Adv. Energy Mater.* **10** 1902467
- [19] Kung P K, Li M-H, Lin P-Y, Jhang J-Y, Pantaler M, Lupascu D C, Grancini G and Chen P 2020 Lead-free double perovskites for perovskite solar cells *Sol. RRL* **4** 1–32
- [20] Maughan A E, Ganose A M, Scanlon D O and Neilson J R 2019 Perspectives and design principles of vacancy-ordered double perovskite halide semiconductors *Chem. Mater.* **31** 1184–95
- [21] Pecunia V, Occhipinti L G, Chakraborty A, Pan Y and Peng Y 2020 Lead-free halide perovskite photovoltaics: challenges, open questions, and opportunities *APL Mater.* **8** 100901
- [22] Perera S et al 2016 Chalcogenide perovskites—an emerging class of ionic semiconductors *Nano Energy* **22** 129–35
- [23] Sun Q, Yin W and Wei S 2020 Searching for stable perovskite solar cell materials using materials genome techniques and high-throughput calculations *J. Mater. Chem. C* **8** 12012–35
- [24] Kuhar K, Crovetto A, Pandey M, Thygesen K S, Seger B, Vesborg P C K, Hansen O, Chorkendorff I and Jacobsen K W 2017 Sulfide perovskites for solar energy conversion applications: computational screening and synthesis of the selected compound LaY₃ *Energy Environ. Sci.* **10** 2579–93
- [25] Goldschmidt V M 1926 Die gesetze der krystallochemie *Naturwissenschaften* **14** 477–85
- [26] Filip M R and Giustino F 2018 The geometric blueprint of perovskites *PNAS* **115** 5397–402
- [27] Li C, Lu X, Ding W, Feng L, Gao Y and Guo Z 2008 Formability of ABX₃ (X = F, Cl, Br, I) halide perovskites *Acta Crystallogr. B* **64** 702–7
- [28] Li Z, Yang M, Park J-S, Wei S-H, Berry J J and Zhu K 2016 Stabilizing perovskite structures by tuning tolerance factor: formation of formamidinium and cesium lead iodide solid-state alloys *Chem. Mater.* **28** 284–92
- [29] Brehm J A, Bennett J W, Schoenberg M R, Grinberg I and Rappe A M 2014 The structural diversity of ABX₃ compounds with d 0 electronic configuration for the B-cation *J. Chem. Phys.* **140** 224703
- [30] Zachariasen W H 1978 Bond lengths in oxygen and halogen compounds of d and f elements *J. Less-Common Met.* **62** 1–7
- [31] Zhang H, Li N, Li K and Xue D 2007 Structural stability and formability of ABO₃-type perovskite compounds *Acta Crystallogr. B* **63** 812–8
- [32] Travis W, Glover E N K, Bronstein H, Scanlon D O and Palgrave R G 2016 On the application of the tolerance factor to inorganic and hybrid halide perovskites: a revised system *Chem. Sci.* **7** 4548–56
- [33] Kieslich G, Sun S and Cheetham A K 2014 Solid-state principles applied to organic–inorganic perovskites: new tricks for an old dog *Chem. Sci.* **5** 4712–5
- [34] Bartel C J, Sutton C, Goldsmith B R, Ouyang R, Musgrave C B, Ghiringhelli L M and Scheffler M 2018 New tolerance factor to predict the stability of perovskite oxides and halides *Sci. Adv.* **5** eaav0693
- [35] Ju M G, Dai J, Ma L and Zeng X C 2017 Perovskite chalcogenides with optimal bandgap and desired optical absorption for photovoltaic devices *Adv. Energy Mater.* **7** 1700216
- [36] Körbel S, Marques M A L and Botti S 2016 Stability and electronic properties of new inorganic perovskites from high-throughput: *ab initio* calculations *J. Mater. Chem. C* **4** 3157–67
- [37] Nishigaki Y et al 2020 Extraordinary strong band-edge absorption in distorted chalcogenide perovskites *Sol. RRL* **4** 1900555
- [38] Comparotto C, Davydova A, Ericson T, Riekehr L, Moro M V, Kubart T and Scragg J 2020 Chalcogenide perovskite BaZrS₃: thin film growth by sputtering and rapid thermal processing *ACS Appl. Energy Mater.* **3** 2762–70
- [39] Wei X, Hui H, Perera S, Sheng A, Watson D F, Sun Y-Y, Jia Q, Zhang S and Zeng H 2020 Ti-alloying of baZrS₃ chalcogenide perovskite for photovoltaics *ACS Omega* **5** 18579–83
- [40] Hanzawa K, Iimura S, Hiramatsu H and Hosono H 2019 Material design of green-light-emitting semiconductors: perovskite-type sulfide SrHfS₃ *J. Am. Chem. Soc.* **141** 5343–9
- [41] Yamaoka S and Okai B 1970 Preparation of BaSnS₃, SrSnS₃ and PbSnS₃ at high pressure *Mater. Res. Bull.* **5** 789–94

- [42] Ravi V K, Yu S H, Rajput P K, Nayak C, Bhattacharyya D, Chung D S and Nag A 2021 Colloidal BaZrS₃ chalcogenide perovskite nanocrystals for thin film device fabrication *Nanoscale* **13** 1616–23
- [43] Wei X et al 2020 Realization of BaZrS₃ chalcogenide perovskite thin films for optoelectronics *Nano Energy* **68** 104317
- [44] Yamaoka S 1972 Synthesis of PbZrS₃ at high pressures *J. Am. Ceram. Soc.* **55** 111
- [45] Wiegers G A, Meetsma A, Haange R J and De Boer J L 1989 Structure of tin hafnium sulfide and lead hafnium sulfide *Acta Crystallogr. C* **45** 847–9
- [46] Schmidt T and Lischka K 1992 Excitation-power dependence of the near-band-edge photoluminescence of semiconductors *Phys. Rev. B* **45** 8989–94
- [47] Jain A et al 2013 Commentary: The Materials Project: a materials genome approach to accelerating materials innovation *APL Mater.* **1** 11002
- [48] Draxl C and Scheffler M 2019 The {NOMAD} laboratory: from data sharing to artificial intelligence *J. Phys. Mater.* **2** 36001
- [49] Carbogno C et al 2020 Numerical quality control for DFT-based materials databases pp 1–7 (arXiv:2008.10402v1)
- [50] Kailkhura B, Gallagher B, Kim S, Hiszpanski A and Han T Y J 2019 Reliable and explainable machine-learning methods for accelerated material discovery *npj Comput. Mater.* **5** 1–9
- [51] Alberi K et al 2019 The 2019 materials by design roadmap
- [52] Kirklin S, Saal J E, Meredig B, Thompson A, Doak J W, Aykol M, Rühl S and Wolverton C 2015 The Open Quantum Materials Database (OQMD): assessing the accuracy of DFT formation energies *npj Comput. Mater.* **1** 15010
- [53] Lejaeghere K et al 2016 Reproducibility in density functional theory calculations of solids *Science* **351** 1415
- [54] Zakutayev A, Wunder N, Schwarting M, Perkins J D, White R, Munch K, Tumas W and Phillips C 2018 An open experimental database for exploring inorganic materials *Sci. Data* **5** 1–12
- [55] Frost J M and Walsh A 2016 What is moving in hybrid halide perovskite solar cells? *Acc. Chem. Res.* **49** 528–35
- [56] Meng W, Saparov B, Hong F, Wang J, Mitzi D B and Yan Y 2016 Alloying and defect control within chalcogenide perovskites for optimized photovoltaic application *Chem. Mater.* **28** 821–9
- [57] Fan Z, Sun K and Wang J 2015 Perovskites for photovoltaics: a combined review of organic-inorganic halide perovskites and ferroelectric oxide perovskites *J. Mater. Chem. A* **3** 18809–28
- [58] Swarnkar A, Mir W J, Chakraborty R, Jagadeeswararao M, Sheikh T and Nag A 2019 Are chalcogenide perovskites an emerging class of semiconductors for optoelectronic properties and solar cell? *Chem. Mater.* **31** 565–75
- [59] Peng Y, Sun Q, Chen H and Yin W J 2019 Disparity of the nature of the band gap between halide and chalcogenide single perovskites for solar cell absorbers *J. Phys. Chem. Lett.* **10** 4566–70
- [60] De Wolf S, Holovsky J, Moon S-J, Löper P, Niesen B, Ledinsky M, Haug F-J, Yum J-H and Ballif C 2014 Organometallic halide perovskites: sharp optical absorption edge and its relation to photovoltaic performance *J. Phys. Chem. Lett.* **5** 1035–9
- [61] Niu S et al 2017 Bandgap control via structural and chemical tuning of transition metal perovskite chalcogenides *Adv. Mater.* **29** 16–21
- [62] Sun Y Y, Agiorgousis M L, Zhang P and Zhang S 2015 Chalcogenide perovskites for photovoltaics *Nano Lett.* **15** 581–5
- [63] Buffiere M, Dhawale D S and El-Mellouhi F 2019 Chalcogenide materials and derivatives for photovoltaic applications *Energy Technol.* **7** 1–17
- [64] Shmidt L 1970 Superconductivity in PbNbS₃ and PbTaS₃ *Phys. Lett.* **31** 551–2
- [65] Crovetto A et al 2019 Shining light on sulfide perovskites: LaYS₃ material properties and solar cells *Chem. Mater.* **31** 3359–69
- [66] Longo G, Degen M J, Sessolo M and Bolink H J 2015 Perovskite solar cells prepared by flash evaporation *Chem. Commun.* **51** 7376–8
- [67] Ahmed E and Ahmed W 2008 Surface engineering of CuIn_{0.75}Ga_{0.25}Se₂ thin films *J. Nano Res.* **2** 69–76
- [68] Pachori R D, Banerjee A and Chopra K L 1986 Flash-evaporated thin films of CuInSe₂ *Bull. Mater. Sci.* **8** 291–6
- [69] Pathak V N, Mistry P, Patel M, Hingarajiya K S, Solaki G K, Pathak V M and Patel K D 2013 Characterization of SnSePb_{0.1} thin films deposited by flash evaporation technique *Adv. Mater. Res.* **665** 311–6
- [70] Orava J, Kohoutek T and Wagner T 2014 Deposition techniques for chalcogenide thin films *Chalcogenide Glasses* ed J L Adam and X Zhang (Cambridge: Woodhead Publishing) pp 265–309
- [71] Lowndes D H, Geohagan D B, Puzosky A A, Norton D P and Rouleau C M 1996 Synthesis of novel thin-film materials by pulsed laser deposition *Science* **273** 898–903
- [72] Chen J, Wang L, Su X, Kong L, Liu G and Zhang X 2010 InGaZnO semiconductor thin film fabricated using pulsed laser deposition *Opt. Express* **18** 1398–405
- [73] Stiff-roberts A D and Ge W 2017 Organic/hybrid thin films deposited by matrix-assisted pulsed laser evaporation (MAPLE) *Appl. Phys. Rev.* **4** 041303
- [74] Ratz T et al 2019 Physical routes for the synthesis of kesterite *J. Phys. Energy* **1** 042003
- [75] Gupta S, Whittles T J, Batra Y, Satsangi V, Krishnamurthy S, Dhanak V R and Mehta B R 2016 A low-cost, sulfurization free approach to control optical and electronic properties of Cu₂ZnSnS₄ via precursor variation *Sol. Energy Mater. Sol. Cells* **157** 820–30
- [76] Hobson T D C, Hutter O S, Fleck N, Daniels L M, Major J D, Ng T M and Durose K 2020 Vegard relation and raman band reference data generated from bulk crystals of kesterite-phase composition series Cu₂ZnSnS_{4-x}Se_{4-4x} (CZTSSe, 0 ≤ x ≤ 1) *Cryst. Growth Des.* **20** 2164–73
- [77] Rudmann D, Brémaud D, Zogg H and Tiwari A N 2005 Na incorporation into Cu(In,Ga)Se₂ for high-efficiency flexible solar cells on polymer foils *J. Appl. Phys.* **97** 84903
- [78] Phillips L J et al 2019 Current enhancement via a TiO₂ window layer for CSS Sb₂Se₃ solar cells: performance limits and high V_{oc} *IEEE J. Photovolt.* **9** 544–51
- [79] Di Giacomo F et al 2015 Flexible perovskite photovoltaic modules and solar cells based on atomic layer deposited compact layers and UV-irradiated TiO₂ scaffolds on plastic substrates *Adv. Energy Mater.* **5** 1–9
- [80] Hösel M and Krebs F C 2012 Large-scale roll-to-roll photonic sintering of flexo printed silver nanoparticle electrodes *J. Mater. Chem.* **22** 15683–8
- [81] Troughton J, Carnie M J, Davies M L, Charbonneau C, Jewell E H, Worsley D A and Watson T M 2016 Photonic flash-annealing of lead halide perovskite solar cells in 1 ms *J. Mater. Chem. A* **4** 3471–6
- [82] Das S, Gu G, Joshi P C, Yang B, Aytug T, Rouleau C M, Geohagan D B and Xiao K 2016 Low thermal budget, photonic-cured compact TiO₂ layers for high-efficiency perovskite solar cells *J. Mater. Chem. A* **4** 9685–90